RESEARCH ARTICLE

Genetic Architecture and Molecular Networks Underlying Leaf Thickness in Desert-Adapted Tomato *Solanum pennellii*

Viktoriya Coneva[1], Margaret H. Frank[1], Maria A. de Luis Balaguer[2], Mao Li[1], Rosangela Sozzani[2], Daniel H. Chitwood [1,3,4]

[1] *Donald Danforth Plant Science Center, 975 North Warson Road, St. Louis, MO 63132, USA*
[2] *Department of Plant and Microbial Biology, North Carolina State University, 2552A Thomas Hall, Raleigh, NC 27695, USA*
[3] *Current address: Independent Researcher, St. Louis, MO USA*
[4] *Corresponding author: Daniel H. Chitwood, dhchitwood@gmail.com*

Short title: Leaf thickness in tomato

One-Sentence Summary: We identified QTL for leaf thickness in desert-adapted tomato and characterized the anatomic and transcriptional alterations associated with this trait using near isogenic lines.

Keywords: leaf thickness, desert adaptation, natural variation, QTL, tomato, gene regulatory networks, leaf development

ABSTRACT

The molecular networks that pattern leaf complexity, lobes, and serrations, have been studied in detail. Our understanding of the genetic underpinnings of leaf thickness, a highly functional quantitative trait, however, is poor. We used a custom-built confocal profilometer to directly measure leaf thickness in a near-isogenic line (IL) population derived from the desert tomato species *Solanum pennellii*, and identified quantitative trait loci (QTL). Significant correlations of leaf thickness with a suite of traits suggest that thickness is patterned in concert with other aspects of leaf morphology. Thicker tomato leaves have dramatically elongated palisade parenchyma cells – a common feature of many thick leaves. To dissect the molecular networks that pattern thickness during leaf development we inferred Dynamic Bayesian Networks of gene expression across early leaf ontogeny (plastochron stages P1-P4) in two ILs with thicker leaves. We identified regulators of *S. pennellii*-like leaf shape and present molecular evidence for alterations in the relative pace of the cellular events underlying leaf development, which may lead to the patterning of thicker leaves. Collectively, these data suggest genetic, anatomical, and molecular mechanisms that pattern leaf thickness in desert-adapted tomato.

INTRODUCTION

Leaves are the primary photosynthetic organs of land plants. Quantitative leaf traits have important connections to their physiological functions, and ultimately, to whole plant productivity and survival. While few aspects of leaf morphology have been unambiguously determined as functional (Nicotra et al., 2011), clear associations between leaf traits and variations in climate have been drawn (Wright et al., 2004). Leaf thickness, the distance between the upper (adaxial) and lower (abaxial) leaf surfaces, has been shown to correlate with environmental variables such as water availability, temperature and light quantity. Thus, on a global scale, across habitats and land plant diversity, plants adapted to arid environments tend to have thicker leaves (Wright et al., 2004; Poorter et al., 2009).

Leaf thickness is a continuous, rather than a categorical, trait. Thus, it is important to distinguish between thickness in the context of "typical" leaf morphology, generally possessing clear dorsiventrality (adaxial/abaxial flattening) in comparison to extremely thick leaves, described as "succulent", which are often more radial. While the definition of succulence is eco-physiological, rather than morphological (Ogburn and Edwards, 2010), at the cellular level it is broadly associated with increased cell size and relative vacuole volume (Gibson, 1982; von Willert et al., 1992). These cellular traits promote the capacity to store water and to survive in dry environments (Becker, 2007). Allometric studies across land plant families have shown that leaf thickness scales specifically with the size of palisade mesophyll cells - the adaxial layer of photosynthetic cells in leaves (Garnier and Laurent, 1994; Roderick et al., 1999; Sack and Frole, 2006; John et al., 2013). Increased palisade cell height leads to increased area of contact with the intercellular space and thereby to improved uptake of carbon dioxide (CO_2) into mesophyll cells (Oguchi et al., 2005; Terashima et al., 2011), possibly offsetting the increased CO_2 diffusion path in thicker leaves. At the organismal level, succulence presents a tradeoff between rapid growth versus drought and heat tolerance (Smith et al., 1997). This idea is supported by global correlations between leaf mass per area (LMA), a

proxy for leaf thickness, and habits associated with slower growth (Poorter et al., 2009).

Although leaf thickness is a highly functional trait, mechanistic understanding of how it is patterned during leaf ontogeny is poor. The main cellular events that underpin leaf development are the establishment of adaxial/abaxial polarity, followed by cell division, directional expansion, and differentiation (Effroni et al., 2008). Changes in the relative timing (heterochrony) and duration of these events can impact leaf morphology, including thickness. Several mutants have been identified that show clear alterations in leaf thickness. These include the Arabidopsis *angustifolia* and *rotundifolia3* (Tsuge et al., 1996), as well as *argonauet1*, *phantastica*, and *phabulosa*, (Bohmert et al., 1998), which have aberrations in the polarity of cell elongation and the establishment of adaxial/abaxial polarity, respectively, as well as the *N. sylvestris fat* and *lam-1* (McHale, 1992, 1993), which affect the extent of periclinal cell division in leaves. However, these developmental mutants do not necessarily inform us of the mechanisms by which natural selection acts to pattern quantitative variation in leaf thickness.

Efforts to understand the genetic basis of leaf thickness in the context of natural variation face several important challenges. First, direct measurement of leaf thickness at a scale that would allow the investigation of Quantitative Trait Loci (QTL) for the trait is not trivial. Because of the difficulty in measuring leaf thickness directly, LMA is most often used as a proxy for this trait (Poorter et al., 2009; Muir et al., 2014). Second, in addition to genetic components, leaf thickness is environmentally plastic – it is responsive to both the quantity and quality of light (Pieruschka and Poorter, 2012). Finally, because leaf thickness varies on a continuous spectrum and is not associated with any particular phylogenetic lineage or growth habit, mechanistic questions regarding its patterning need to be addressed in a taxon-specific manner.

With these considerations in mind, we used two members of the tomato clade (*Solanum* sect. *Lycopersicon*)**,** which are closely related, morphologically distinct, and occupying distinct environments (Nakazato et al., 2010) to study the genetic basis and

developmental patterning of leaf thickness. The domesticated tomato species *S. lycopersicum* inhabits a relatively wide geographic range characterized by warm, wet conditions with little seasonal variation. By contrast, the wild species *S. pennellii* is endemic to coastal regions of the Atacama desert of Peru, a habitat characterized by extremely dry conditions (Nakazato, et al., 2010). The leaves of *S. pennellii* plants, therefore, exhibit morphological and anatomical features that are likely adaptations to dry conditions (McDowell et al., 2011; Haliński et al., 2015), including thick leaves (Koenig et al., 2013). Moreover, a set of homozygous introgression lines (ILs) harboring defined, partially overlapping segments of the *S. pennellii* genome in an otherwise *S. lycopersicum* background (Eshed and Zamir 1995) has been used to successfully map a number of QTL, including fruit metabolite concentrations (Fridman et al., 2004; Schauer et al., 2006), yield (Semel et al., 2006), and leaf shape (Chitwood et al., 2013). Here, we used a custom-built dual confocal profilometer to obtain precise measurements of leaf thickness across the IL panel and identified QTL for this trait in tomato. Leaf thickness correlates with other facets of leaf shape, as well as a suite of traits associated with desiccation tolerance and lower productivity. We investigated the anatomical manifestations of thickness in tomato and found a prominent increase in palisade cell height. Finally, we inferred comparative gene regulatory networks of early leaf development (plastochron stages P1-P4) in two thick lines using organ-specific RNA-Seq and identified molecular networks that pattern *S. pennellii*-like desert-adapted leaves.

RESULTS

Complex genetic architecture of leaf thickness and shape across *S. pennellii* ILs

To investigate the genetic architecture and patterning of leaf thickness in the *S. pennellii* IL panel, we used a custom-built dual confocal profilometer device (Supplemental Figure 1), which generates precise thickness measurements throughout the leaflet lamina at a range of resolutions (0.1 - 1.0 mm^2) and at high-throughput rates. The device makes use of two confocal lasers positioned on either side of the sample and calculates thickness by measuring the distance between each of the sample's surfaces and the corresponding laser

probe. Finally, we visualize thickness as a heatmap of thickness values across the surface of the leaf lamina (Figure 1).

We first compared leaflet thickness in *S. lycopersicum* var. M82 and its desert relative *S. pennellii* LA0716. Our confocal profilometer measurements showed that *S. pennellii* leaflets are thicker than those of domesticated tomato, as previously reported (Figure 1, Koenig et al., 2013), demonstrating the capacity of this device to quantitatively detect fine differences in leaf lamina thickness. We then measured leaf thickness across the *S. pennellii* introgression line panel in field conditions.

We used mixed linear regression models to compare each of the introgression lines to the domesticated parent M82 (Supplemental Dataset 1) and found that 31 ILs had significantly thicker leaflets than the M82 parent, while 5 had transgressively thinner leaflets. The overall broad-sense heritability for leaflet thickness is 39.1% (Figure 2). The lines with thickest leaflets are IL5-4, IL5-3, IL8-1, IL4-3, IL8-1-1 (contained within IL8-1), and IL2-5, while IL4-1-1, IL2-6-5, IL9-1-3, IL12-4-1, and IL2-1 have thinner leaves than the M82 parent. We compared our field experiment with leaf thickness data for greenhouse-grown plants. We selected 20 ILs, which were highly significant for leaf thickness differences from M82 in field conditions ($p < 0.001$) and observed that only some of these lines are also significantly thicker than the domesticated parent in greenhouse conditions ($p < 0.05$, Supplemental Figure 2).

For each leaflet in our field experiment, we also quantified leaf mass per unit area (LMA), which reflects both thickness and density, and is traditionally used as a proxy for leaf thickness. Although the heritability for LMA is similar to that for thickness (33.2% and 39.1%, respectively), significant QTL for these two traits do not consistently overlap (Supplemental Table 1).

We scanned the outlines of each leaflet and extracted shape features: aspect ratio, roundness, circularity and solidity. Similar to thickness, we determined QTL for leaflet

circularity – the ratio between leaflet area and the square of its perimeter – which increases with decreasing leaflet lobing and serration. The heritability of this trait is 50.2% and we detected a total of 43 ILs with significantly higher circularity than M82, reflecting decreased margin elaboration. Among these lines, IL4-3 has the strongest phenotype (circularity = 0.673), while the partially overlapping ILs 4-2 and 4-4 also have high circularity values (0.615 and 0.555, respectively compared with 0.440 for M82)(Figure 2B).

Leaf thickness and LMA are correlated with distinct suites of traits in tomato

We generated pairwise correlations between leaflet thickness, LMA, and a suite of other previously published traits including metabolite (MET), morphological (MOR), enzymatic activity in fruit pericarp (ENZ), seed-related (SED), developmental (DEV), and elemental profile-related (ION) (Supplemental Datasets 2-4, Chitwood et al., 2013 and references therein). Spearman's correlation coefficients with significant q-values ($q < 0.050$) are reported in Figure 2C. Leaf thickness and LMA are correlated (rho = 0.423, q = 0.003). Leaf thickness also correlates with leaf shape parameters, such as roundness (rho = 0.328, q = 0.044), aspect ratio (rho = -0.327, q = 0.045), and the first two principal components of the elliptical Fourier descriptors of leaflet shape (EFD.PC1 rho = 0.414, q = 0.004 and EFD.PC2 rho = 0.406, q = 0.005). Thickness is negatively correlated with several reproductive traits, including yield (rho = -0.337, q = 0.037), seed weight (rho = -0.342, q = 0.033) and seed number per plant (rho = -0.339, q = 0.036). Moreover, leaf thickness is negatively correlated with leaf stomatal ratio, the relative density of stomata on the abaxial and adaxial sides of the leaf (rho=-0.352, q = 0.031), and positively with Glutamate dehydrogenase activity (rho = 0.367, q = 0.017) and seed galactinol content (rho = 0.342, q = 0.048).

Leaf mass per area is associated with a distinct suite of traits from leaf thickness. In addition to a positive correlation with the content of some enzymes (GAPDH and Shikimate DE) and metabolites (Glutamate), LMA is significantly negatively correlated with the accumulation of ^{23}Na and ^{25}Mg in all leaflets tested. LMA, but not leaf

thickness, is also significantly positively correlated with total plant weight, reflecting vegetative biomass accumulation.

Thick IL leaves have elongated palisade parenchyma cells

Leaf cross-sections of field-grown M82 and select ILs with increased leaf thickness, as well as greenhouse-grown *S. pennellii* (Sp) leaves were stained with propidium iodide to assess the anatomical changes that lead to increased leaf thickness. We observed that, relative to the M82 parent, the Sp parent and several ILs, have an elongated palisade parenchyma cell layer corresponding to the adaxial layer of photosynthesizing cells in tomato leaves (Figure 3). Palisade parenchyma elongation is especially dramatic for IL1-3, IL2-5, IL4-3, and IL10-3. We thus extended detailed further analyses to IL2-5 and IL4-3. In addition to increased leaf thickness, IL4-3 was also of interest due to its pronounced leaflet shape phenotype (Figure 2B, Figure 3C).

First, we wanted to know the approximate developmental timing of leaf thickness patterning during leaf ontogeny. Using a DR5::Venus reporter, which marks emerging leaf and leaflet primordia in tomato (Ben-Gera et al., 2012), we observed that IL2-5 and IL4-3 leaves begin to look different from M82 around the plastochron 3 (P3) stage of leaf development. IL2-5 P3 leaf primordia have more pronounced leaflet primordia as visualized by Venus fluorescence foci, while IL4-3 crossed with DR5::Venus shows a single leaflet primordium at P3 (Figure 3D-F). Next, we quantified P3 organ dimensions and compared them with the M82 parental line. For this, we assembled 3D confocal reconstructions of vegetative shoot apices, calculated the surface mesh, extracted P3 leaf primordia, and quantified their total volume, length, and mean diameter. We found that IL4-3 P3 leaf primordia are significantly larger than M82 in terms of overall volume ($p = 0.0179$), as well as both length ($p = 0.0035$) and diameter ($p = 0.0230$). In IL2-5 increased P3 volume and diameter are not statistically significant, while length is comparable to M82 (Figure 3G).

Transcriptomic signatures of early leaf development in thicker ILs

To investigate the molecular events that define the patterning of IL2-5 and IL4-3 leaves, we isolated leaf primordia from each IL and the two parents (M82 or Sl and Sp) at four successive stages of development: P1 (containing the shoot apical meristem, SAM, and the youngest leaf primordium), P2, P3 (characterized by leaflet emergence) and P4 (typically the onset of cell differentiation) (Figure 4A). For *S. pennellii*, P1 samples were comprised of the SAM, P1, and P2, since these organs were not separable by hand dissection. Thus, the Sp transcriptomic dataset includes samples designated as P1, P3, and P4. Principal Component Analysis (PCA) of the resulting RNA-Seq data, after normalization and filtering, shows that samples group clearly by organ stage (PC2) (Figure 4B). In addition, PC1 separates *S. pennellii* samples from all other genotypes. To investigate how IL leaves are similar to the Sp parent, we looked for genes that are differentially expressed (DEGs) between corresponding stages of each IL and the M82 parent, while also being differentially expressed between M82 and Sp. In other words, we identified the set of DEG for each organ stage that is common to each IL and Sp relative to M82. For P2 we considered only the comparison with M82, as our Sp dataset did not include independently dissected P2 stage primordium samples (Supplemental Figure 3, Supplemental Dataset 5).

We identified a total of 812 DEGs across P1-P4 stages in IL2-5, and of these, 544 are up-regulated in at least one organ stage, while 269 are down-regulated (Figure 4C). In IL4-3, we detected 632 DEG, 361 of which are up-regulated and 271 are down-regulated in the IL (Figure 4D). Many of the DEGs are differentially expressed at more than one stage (Supplemental Figure 3, Supplemental Dataset 5). Additionally, based on tomato transcription factor (TF) annotation by Suresh et al. (2014), we identified putative transcription factor-encoding genes among each IL's DEG sets. Myb-related, Ethylene Responsive, MADS, and WRKY are the abundant classes of TF-encoding DEGs in IL2-5, while in IL4-3 TFs belonging to bZIP and Myb-related are highly represented families (Supplemental Figure 4). We identified differentially expressed TF-encoding genes that are common to the two ILs and the Sp parent (Figure 4E), reasoning that some of these can be regulators of leaf thickness. Five of the seven shared TF-encoding genes are up-

regulated in the ILs relative to M82. A MADS-box TF (Solyc12g087830) is up-regulated at all stages in both ILs. The GRAS TF Solyc08g014030 is up-regulated at P2 in both ILs, while its expression increases at each progressive stage and peaks at P4 in all genotypes.

To compare trends in cellular and developmental events during leaf ontogeny among genotypes, we explored expression patterns of Mapman-annotated functional categories associated with cell proliferation and cell differentiation (Thimm et al., 2004) (Figure 5). The expression profiles of cell cycle and cell division associated genes are distinct for both IL2-5 and IL4-3 relative to M82. In IL2-5 cell cycle-associated genes peak in expression at P3, while in IL4-3 the expression of these genes progressively decreases from P1 to P4. Moreover, the expression of the leaf maturation TCP transcription factor-encoding gene *LANCEOLATE* (Solyc07g062680) is higher in P3 primordia of IL2-5 (Supplemental Figure 5). The expression of photosynthesis-associated transcripts is also higher at P3 in this IL relative to both M82 and IL4-3.

Next, we applied GO enrichment analysis on DEGs in each organ using agriGO (Du et al., 2010) (Supplemental Dataset 6). At P4, the set of up-regulated genes in IL2-5 is enriched for biological process terms relating to “photosynthesis“ (GO:0015979) and “translation” (GO:0006412), while down-regulated genes at this stage are enriched for terms relating to “DNA binding” (GO:0003677). IL4-3 P2 up-regulated genes are significantly associated with “cysteine-type peptidase activity“ (GO:0008234).

To broadly characterize the types of processes that may regulate the molecular networks of early leaf development in the ILs, we identified statistically enriched promoter motifs among the organ-specific DEG sets (Figure 6, Supplemental Dataset 7). Promoter motifs associated with regulation by abiotic factors such as light, circadian clock, water availability, and temperature are prominent among IL2-5 genes. In addition, binding sites for developmental regulators, hormone-associated promoter motifs, and a cell cycle regulator are among the list of significant motifs. Among development-associated motifs,

CArG (MADS-box), BEL1-like (BELL) and SBP-box transcription factor binding sites are also significantly enriched in both IL 2-5 and 4-3 DEG sets. (Figure 6, Supplemental Dataset 7).

Gene regulatory networks of early leaf development in thick ILs

To detect regulators of early leaf development that each IL (IL2-5 and IL4-3) shares with the *S. pennellii* parent, we inferred Dynamic Bayesian Networks (DBN) using the IL and Sp overlapping DEG sets described in the previous section. Additionally, we only allowed putative transcription factor-encoding genes (Suresh et al., 2014) as "source" nodes (genes that control the expression of other co-expressed genes). First, we constructed individual networks for each leaf developmental stage, for which an overlap with Sp data is available (P1, P3, P4), and then combined the results to visualize the overall *S. pennellii*-like leaf developmental networks (Figure 7, Supplemental Dataset 8). The IL2-5 network (Figure 7A) contains two major regulators, which are central to more than one developmental stage: a SQUAMOSA promoter-binding protein-like domain gene (SBP-box 04g, Solyc04g064470) (Figure 7B) and a CONSTANS-like Zinc finger (Zn-finger CO-like 05g, Solyc05g009310) (Supplemental Dataset 8). Similarly, the IL4-3 network (Figure 7C) features two central regulators: a BEL1-like homeodomain transcription factor gene (BEL1 04g, Solyc04g080780) (Figure 7D) and a MADS-box domain-containing gene (MADS-box 12g, Solyc12g087830) (Supplemental Dataset 8).

We also inferred a second set of networks for each of the ILs by identifying DEGs using similar criteria as above. However, in contrast to the previous set of networks, where genes were separated into organ stages based on differential expression at each discrete stage, we used a clustering approach to group regulators and select co-expressed gene sets according to expression profiles. For these analyses, we also included P2 DEGs (IL vs M82) to ensure continuity of expression profiles (Supplemental Dataset 9). This approach allowed us to examine a more dynamic view of early developmental processes. The resulting networks (Supplemental Dataset 9) feature a putative auxin responsive TF AUX/IAA 12g (Solyc12g096980) for both ILs (Figure 7E, F). Moreover, the AUX/IAA

12g sub-network or IL2-5 includes the GRAS domain TF that is up-regulated during leaf development in both ILs (GRAS 08g, Solyc08g014030) (Figure 4E, Figure 7E).

DISCUSSION

Leaf thickness has a complex genetic architecture in desert-adapted tomato and is associated with overall leaf shape, desiccation tolerance, and decreased yield

While extensive progress has been made dissecting the molecular-genetic patterning of two-dimensional leaf morphology, relatively little is known about the third dimension of leaf shape – thickness. Here, we used a custom-built dual confocal profilometer to obtain direct measurements of leaf thickness across the *S. pennellii* x *S. lycopersicum* IL panel (Eshed and Zamir, 1995) (Figure 1, Supplemental Figure 1) and identified QTL for this trait (Figure 2A). We found that nearly half of the ILs have significantly thicker leaves than the domesticated parent M82, while a small number have transgressively thinner leaves. The broad-sense heritability for leaf thickness in this experiment is moderate (39%). Collectively, these observations point to a complex genetic basis for this trait. A previous quantitative genetic analysis of a suite of desert-adaptive traits in the same *S. pennellii* IL panel found fewer significantly thicker lines and lower heritability (12%) for this trait (Muir et al., 2014). However, the previous study estimated thickness as the ratio of LMA to leaflet dry matter content, while we measured thickness directly. Further, our study was conducted in field conditions, while Muir et al. (2014) measured the trait using greenhouse-grown plants. Given that environment significantly affects the magnitude of this trait (Supplemental Figure 2) it is not surprising that these studies report only partially overlapping outcomes.

In order to understand how variation in leaf thickness relates to other traits, particularly to leaf mass per area, we calculated pairwise correlation coefficients among all leaf shape and elemental profile traits, as well as a collection of previously published traits (summarized in Chitwood et al., 2013; Supplemental Datasets S3, S4). As expected, leaf thickness and LMA are significantly correlated across the IL panel. However, the two

have distinct sets of significant trait correlations (Figure 2C). Collectively, these data suggest that thickness and LMA are likely patterned by separate mechanisms and that direct measurements of leaf thickness are necessary to further dissect the genetic basis of this trait.

Leaf thickness is significantly correlated with leaf shape traits such as aspect ratio and the first two principal components of elliptical Fourier descriptors of overall shape. However, our data do not establish whether this correlation reflects a common patterning mechanism or developmental and/or mechanical constraints among these traits. Alternatively, the relatively modest correlations (rho values between 0.33 - 0.41) could reflect independent variation in these traits resulting in considerable flexibility in final leaf morphology, as suggested by Muir et al. (2016).

Leaf thickness is negatively correlated with yield-related traits, which suggests a trade-off between investments in vegetative and reproductive biomass that is further substantiated by the positive correlation between LMA and plant weight (Figure 2C). Some studies support the hypothesis of a tradeoff between leaf mass per area and rapid growth (Smith et al., 1997; Poorter et al., 2009), while others find poor coordination between growth rate and LMA (Muir et al., 2016). Finally, leaf thickness is significantly correlated with leaf stomatal ratio, Glutamate dehydrogenase activity, and galactinol content in seeds, a suite of traits associated with desiccation tolerance in plants (Taji et al., 2002; Lightfoot et al., 2007). We also observed negative correlations between LMA and the accumulation of several elements in leaves, most notably ^{23}Na and ^{25}Mg (Figure 2C). This finding supports the idea that LMA and thickness are distinct traits, and that LMA reflects the material composition of leaves, while leaf thickness is a developmentally patterned trait.

Thicker *S. pennellii* IL leaves have elongated palisade parenchyma cells

The observed elongated palisade parenchyma cells in the leaves of several ILs with significantly thicker leaves (Figure 3A), as well as in the desert-adapted *S. pennellii* parent suggest that leaf thickness is accomplished by directional expansion of a single

cell type in leaves – the palisade parenchyma. Palisade cell height is positively correlated with photosynthetic efficiency (Niinemets et al., 2009; Terashima et al., 2011) and water storage capacity in succulent CAM (Crassulacean Acid Metabolism) plants (Nelson et al., 2005). Thus, taller palisade cells may be a direct adaptation to dry environments. Consistent with this adaptive hypothesis, IL2-5 is drought tolerant (Gong et al., 2010). Further, IL2-5 DEG promoters are enriched in motifs that reflect responsiveness to abiotic stimuli, prominently light and water status (Figure 6, Supplemental Dataset 7). Leaf thickness is known to be responsive to both light quality and quantity in Arabidopsis (Poorter et al., 2009; Wuyts et al., 2012; Kalve et al., 2014). Taken together with our data, which compares greenhouse to field-grown plants (Supplemental Figure S2), these observations highlight an important role of environmental cues during leaf development for the patterning of thickness and palisade cell height.

Early leaf development is distinct in IL2-5, IL4-3, and the domesticated parent

Using an auxin reporter line, which marks emerging leaflet primordia (Koenig et al., 2009; Ben-Gera et al., 2012), we observed differences in the developmental timing of leaflet initiation at the P3 stage between ILs 2-5 and 4-3, and M82 (Figure 3D-F). IL4-3 P3 leaves have fewer leaflet primordia, while the length, average diameter, and overall volume of P3 laves are increased relative to M82 (Figure 3D-G). In contrast, leaflet development appears advanced in IL2-5 P3 and overall organ volume is larger than for M82, albeit not significantly (Figure 3D-G). These observations suggest that leaf thickness and shape are the result of changes in the timing and extent of cellular events during leaf ontogeny in these ILs. A partially overlapping series of cell division, cell expansion, and cell differentiation events underlie leaf development (Effroni et al., 2008). These processes are tightly coordinated to buffer perturbations in overall organ shape and size (Tsukaya 2003; Beemster et al., 2003). Thus, the relative timing and duration of any of these events can impact leaf morphology. Consistent with this idea, our results suggest that increased leaf thickness and palisade cell height in IL2-5 and IL4-3 are patterned by distinct cellular dynamics during leaf development compared to the domesticated parent.

For example, in IL4-3 a general decrease in cell cycle/cell division gene expression starting early in leaf ontogeny (Figure 5) could lead to increased cell elongation later in ontogeny similar to observations in Arabidopsis leaf development (Wuyts et al., 2012). Thicker leaves and highly elongated palisade parenchyma cells in mature leaves could mechanistically result from this hypothetical sequence of cellular events. In IL2-5, on the other hand, cell proliferation-associated gene expression peaks at P3 (Figure 5), suggesting a distinct trajectory of leaf development in this line.

Additional evidence for alterations in cell proliferative activity in these thick ILs is the fact that the GRAS-domain TF GRAS 08g (Solyc08g014030) is up-regulated in both lines (Figure 4E, Supplemental Dataset 5). This gene is closely related to the Arabidopsis gene encoding SHORTROOT (SHR) (Huang et al., 2015), which together with another GRAS-domain TF, SCARECROW (SCR), regulates the duration of cell proliferation in leaves (Dhondt et al., 2010). Moreover, consistent with previous reports, IL2-5 and IL4-3 DEGs are enriched for E2F binding site motifs (Supplemental Dataset 7, Ranjan et al., 2016). E2F transcription factors act downstream of SHR and SCR to regulate progression through the S-phase of the cell cycle (Dhondt et al., 2010). These data support the notion that the extent and/or duration of cell proliferation underpin increased thickness in these lines. While cell-level dynamics associated with leaf development have been profiled in some detail in Arabidopsis (Andriankaja et al., 2012; Gonzalez et al., 2012), no such analyses have been performed for the development of compound leaves.

Finally, it is conceivable that palisade cell-specific regulators of cell division may modulate leaf thickness as is the case for Arabidopsis leaves, where increased anticlinal cell expansion of the palisade mesophyll is paired with lower division rates in these cells relative to epidermal cells (Wuyts et al., 2012; Kalve et al., 2014).

Gene networks point to a role for the pace of leaf ontogeny in leaf thickness patterning in IL2-5

Our gene expression data suggest that the pace of IL2-5 leaf development may be altered.

Transcript accumulation of the leaf differentiation promoting CIN-TCP transcription factor-encoding gene *LANCEOLATE* (Ori et al., 2007; Schleizer-Burko et al., 2011) is higher in P3 primordia of IL2-5 relative to M82 (Supplemental Figure 5) consistent with alteration in the pace of leaf differentiation in this IL. Further, an SBP-box domain gene, SBP 04g (Solyc04g064470) is both highly expressed throughout leaf development in IL2-5 and is central to gene regulatory networks in this IL (Supplemental Figure 3, Figure 6B). SBP transcription factors regulate various aspects of plant growth by controlling the rate and timing of developmental events, including the transition from juvenile to adult leaf identity, flowering time, and leaf initiation rate (reviewed in Preston and Hileman, 2013). The promoters of IL2-5 DEGs are enriched for SQUAMOSA promoter binding protein (SBP) motifs (Supplemental Dataset 7) supporting the central role of this group of transcription factors during IL2-5 leaf ontogeny.

We observed differences in the timing and degree of transcript accumulation for the MADS-box transcription factor MBP20/AGL79 (Solyc02g089210) (Supplemental Figure 4). MBP20/AGL79 is negatively regulated by LANCEOLATE, and is thus a direct readout of the leaf differentiation program in tomato (Burko et al., 2013). *MBP20/AGL79* is expressed precociously in IL2-5 (Supplemental Figure 4) and consistent with its role in promoting leaflet initiation (Burko et al., 2013), we observe that P3 stage leaves have larger, i.e. developmentally advanced leaflets relative to M82 (Figure 3C, D).

Finally, GO terms for “photosynthesis” and “translation” are enriched among P4 up-regulated genes. This observation shows that processes associated with cell differentiation (i.e. photosynthetic gene function and protein translation) are precociously activated in IL2-5 and supports our hypothesis that the overall schedule of leaf developmental events is hastened in this line.

Molecular evidence points to novel regulators of leaf shape in tomato

In addition to having thicker leaves and elongated parenchyma, IL4-3 harbors previously reported major QTL for leaf shape (Holtan and Hake, 2003; Chitwood et al., 2013). Like

460 *S. pennellii*, IL4-3 leaflets have significantly smoother margins (fewer serrations) than
461 M82 (Figure 3C), as reflected in increased circularity (Figure 2B). The heritability of this
462 trait is high (50.2%) suggesting a strong genetic basis. Gene expression data for IL4-3
463 highlight a central role for BEL1-like homeodomain TFs during leaf development. First,
464 promoters of IL4-3 DEG are enriched for BEL-like motifs at several developmental
465 stages (Figure 6, Supplemental Dataset 7). Two genes encoding BEL1-like proteins
466 (also referred to as TALE for Three Amino acid Loop Extension), both in *cis* to IL4-3,
467 are among the up-regulated genes in this line - *SAWTOOTH1* (*SlSAW1*, Solyc04g079830)
468 and *SlBEL11* (BEL1 04g, Solyc04g080780) (Supplemental Figure 4, Supplemental
469 Dataset 5). In addition, *SlBEL11* is a central node in the organ-specific regulatory
470 network of IL4-3 (Figure 7D). BEL1-like homeodomain proteins interact with class I
471 KNOX transcription factors to pattern the SAM and lateral organs, including leaf
472 complexity (Kimura et al., 2008; Hay and Tsiantis, 2010) and the extent of lobing and
473 serrations (Kumar et al., 2007). Thus, up-regulation of *SlSAW1* and *SlBEL11* suggest
474 possible mechanisms for the observed increase in leaflet circularity in IL4-3 (Figure 2B),
475 whereby BEL1-like protein interactions with KNOX proteins in the margins of leaves
476 result in decreased leaflet and leaf complexity in this line.
477
478 Finally, the enrichment of GO terms associated with “cysteine-type peptidase activity”
479 among DEGs in IL4-3 (Supplemental Dataset 6) is consistent with previous reports
480 highlighting a central role for this functional category in IL4-3 and *S. pennellii* (Ranjan et
481 al., 2016; Ichihashi et al., 2014). While cysteine peptidases have been shown to be
482 important during leaf senescence (Diaz-Mendoza et al., 2014), it is possible that, given
483 the distinct Sp-like leaflet shape of IL4-3, cysteine-peptidase activity may be involved in
484 patterning leaf shape in this IL.
485
486 **MATERIALS AND METHODS**
487
488 **Plant material and growth conditions**
489 Seeds for 76 *S. pennellii* introgression lines (LA4028-LA4103; Eshed and Zamir, 1995)

and the *S. lycopersicum* domesticated variety M82 (LA3475) were obtained either from Dr. Neelima Sinha (University of California, Davis) or from the Tomato Genetics Resource Center (University of California, Davis). All seeds were treated with 50% bleach for 3 min, rinsed with water and germinated in Phytatrays (P1552, Sigma-Aldrich). Seeds were left in the dark for 3 days, followed by 3 days in light, and finally transferred to greenhouse conditions in 50-plug trays. Hardened plants were transplanted to field conditions at the Bradford Research Station in Columbia, MO (May 21, 2014) with 3 m between rows and about 1 m spacing between plants within rows. A non-experimental M82 plant was placed at both ends of each row, and an entire row was placed at each end of the field to reduce border effects on experimental plants. The final design had 15 blocks, each consisting of 4 rows with 20 plants per row. Each of the 76 ILs and 2 experimental M82 plants were randomized within each block. IL6-2 was excluded from final analyses due to seed stock contamination. For the analysis of leaf primordia by confocal microscopy and RNA-Seq, IL2-5, IL4-3, M82, and *S. pennellii* seeds were germinated as above and transferred to pots in controlled growth chamber conditions: irradiance at 400 μmol/m^2/s, 23 ^{o}C, 14-hour days. Growth conditions for the drought phenotyping experiment were irradiance of 200 μmol/m^2/s at a daytime temperature of 22 ^{o}C and 18 ^{o}C at night.

Whole-plant phenotyping under drought

The LemnaTec Scanalyzer plant phenotyping facility at the Donald Danforth Plant Science Center (LemnaTec GmbH, Aachen, Germany) was used to phenotype approximately 3-week old *S. lycopersicum* and *S. pennellii* plants (n = 8/genotype) subjected to one of three watering regimes: 40 % field capacity, 20 % field capacity, and no watering (0 % field capacity). Top view images of each plant taken every second night over 16 nights were analyzed using custom pipelines in Lemna Launcher (LemnaTec software) to extract total plant pixel area (a proxy for biomass).

Trait measurements

After flowering (July 2014), four fully expanded adult leaves were harvested from each

plant; the adaxial (upper) surfaces of distal lateral leaflets harvested from the left side of the rachis were scanned with a flatbed scanner to obtain raw JPG files. The middle portion of each leaflet was then attached on a custom-build dual confocal profilometer device (Supplemental Figure 1) and the thickness of each leaflet was measured across the leaflet surface at a resolution of 1 mm^2. Median thickness was calculated across each leaflet using values in the range (0 mm < thickness < 2 mm) and these median values were averaged across four leaflets per plant to arrive at a single robust metric of leaf thickness. Finally, entire leaflets were dried and their dry mass used to calculate leaf mass per area (LMA) for each leaflet. Leaflet outline scans were processed using custom macros in Image J (Abramoff et al., 2004) to segment individual leaflets and to threshold and binarize each leaflet image. Shape descriptors area, aspect ratio, roundness, circularity, and solidity (described in detail in Chitwood et al., 2013) were extracted from binary images. Additionally, elliptical Fourier descriptors (EFDs) for leaflet outlines were determined using SHAPE (Iwata and Ukai, 2002). For this analysis 20 harmonics with 4 coefficients each were used to derive principal components (PC) that describe major trends in the shape data.

Elemental profiling (ionomics)

Distal lateral leaflets of fully expanded young (Y) and old (O) leaves of the same plants as above were collected from five individuals of each genotype. Whole leaflets were weighed and digested in nitric acid at 100 ^oC for 3 hours. Elemental concentrations were measured using an inductively coupled plasma mass spectrometer (ICP-MS, Elan DRC-e, Perkin Elmer) following the procedure described in Ziegler et al. (2012). Instrument reported concentrations were corrected for losses during sample preparation and changes in instrument response during analysis using Yttrium and Indium internal standards and a matrix-matched control run every tenth sample. Final concentrations were normalized to sample weight and reported in mg analyte per kilogram tissue.

Statistical analyses and data visualization

All statistical analysis and visualization was carried out using R packages (R Core Team,

2013). QTL were identified using the mixed effect linear model packages lme4 (Bates et al., 2014) and lmerTest (Kuznetsova et al., 2015) with M82 as intercept, IL genotype as a fixed effect, and field position attributes (block, row, and column) as random effects. Only effects with significant variance ($p < 0.05$) were included in the final models. For elemental composition data, leaf age ("young" and "old") was also included as a random effect unless the variance due to age was the greatest source of variance; in such cases, young and old samples were analyzed separately. Heritability values represent the relative proportion of variance due to genotype. For the quantification of organ volume parameters and photosynthesis measurements, linear models were used to test the effect of genotype. All plots were generated with the package ggplot2 (Wickham, 2009).

Trait correlations and hierarchical clustering

For trait correlation analyses we included all traits reported in this study and measured on the same set of field-grown IL individuals (leaf thickness, LMA, leaflet shape traits, elemental profiles). We also included several sets of meta-data detailed in Supplemental Dataset 3, including DEV (developmental), MOR (morphological), MET (fruit pericarp metabolite content), ENZ (enzyme activity), and SED (seed metabolite content) related traits (from Chitwood et al., 2013 and references within). Spearman correlation coefficients (rho) were calculated between each pair of traits using the rcorr function in Hmisc (Harrell et al., 2015) and p-values for the correlations were corrected for False Discovery Rate using Benjamini Hochberg (Supplemental Dataset 4). Hierarchical clustering and visualization of significant correlation ($q < 0.05$) of leaf thickness and LMA were clustered (hierarchical "ward" algorithm) and visualized using pheatmap (Kolde, 2015).

Confocal microscopy, 3D-reconstructions, and organ volume quantification

For mature leaf cross-sections, field-grown leaves were fixed in FAA (4 % formaldehyde, 5 % glacial acetic acid, 50 % ethanol), vacuum infiltrated, dehydrated through an ethanol series, rehydrated to 100 % water, stained in 0.002 % propidium iodide (Thermo Fisher, P21493) for 2 hours, dehydrated to 100 % ethanol, and finally cleared in 100 % methyl

salicylate (Sigma, M6752) for 7 days. Hand-sections were visualized with a Leica SP8 laser scanning confocal microscope using white light laser excitation at 514 nm with a 20X objective. Two partially overlapping images were captured for each cross-section and merged into a single image using the "Photomerge" function in Adobe Photoshop CC 2014 (Adobe Systems Incorporated). For the quantification of P3 leaf primordium dimensions, shoot apices (shoot apical meristem and P1-P4) of 14 day-old seedlings grown in controlled conditions were excised, fixed, processed, and stained as detailed for leaf cross sections above. Confocal stacks were obtained at software-optimized intervals, and exported as TIFF files. Raw stack files were imported into MorphoGraphX (Reulle et al., 2015). After Gaussian filtering, the marching cubes surface reconstruction function was used (cube size = 5 μm and threshold = 7,000). The resulting surface mesh was smoothed and subdivided twice and exported as a PLY file. To minimize the effects of trichomes on P3 volume, all meshes were trimmed in MeshLab (Cignoni et al., 2008). Volume, length, and diameter of processed P3 meshes were calculated using custom scripts in MatLab (MathWorks, Inc.). Briefly, first, we detected the boundary of each hole and calculated its centroid point. We connected boundary points of each hole to its centroid and filled the triangle faces. After filling all the holes, 3D mesh represents the closed surface. Then we calculated the volume based on the divergence theorem, which makes use of the fact that the inside fluid expansion equals the flux ($\vec{F}$) of the fluid out of the surface (S). When the flux is $\vec{F} = (x, 0,0)$, the volume is $V = \oiint (\vec{F} \cdot \vec{n})\, dS$, where $\vec{n}$ is normal vector. Thus, for each triangle, we computed the normal vector $\vec{n} = (x_n, y_n, z_n)$, the area A, and the centroid point $P = (x_p, y_p, z_p)$. The volume V is the summation of $Ax_n x_p$ for all triangles. To estimate organ arch length we made use of the fact that the Laplace-Beltrami eigenfunctions are deformation invariant shape descriptor (Rustamov, 2007). We thus employed its first eigenfunction, which is associated with the smallest positive eigenvalue and discretized the eigenfunction values into 50 sets to compute the centroid point to each set. We fit a cubic function by fixing two end-point constraints to those centroid points to get a smooth principle median axis. Note that the two end points were manually adjusted to correct for artifacts. The length of this axis is

used to quantify the length of the organ. Finally, we calculated mean organ diameter as $d = 2\sqrt{\frac{V}{\pi L}}$. Visualization of the auxin reporter DR5::Venus (Ben-Gera et al., 2012) crossed to M82, IL2-5, and IL4-3 was performed on live 14 day-old shoot apices (SAM-P3). Samples (6 per genotype) were visualized with a Leica SP8 confocal microscope as detailed for PI-stained apices above; emission spectra were collected for the Venus fluorophore and chlorophyll auto-fluorescence separately. Image stacks were exported as TIFF files and processed in Image J to produce 3D projections combining fluorescence from the Venus and chlorophyll channels.

RNA-Seq library preparation and sequencing

Apices of fourteen day-old IL2-5, IL4-3, M82, and *S. pennellii* (Sp) plants grown in a randomized design under controlled growth conditions were hand-dissected under a dissecting microscope to separate plastochrons P4, P3, P2, and P1+SAM organs corresponding approximately to leaves L5 – L8. For Sp plants we were not able to separate P2 primordia from the apex and so we obtained P4, P3, and SAM+P1+P2 samples. Dissected organs were removed from the apex in less than 60 seconds and immediately fixed in 100 % ice-cold acetone to preserve the integrity of RNA in the sample. Each biological replicate is a pool of 10 individuals, and a total of 5 biological replicates were obtained for each genotype/organ combination. RNA was extracted using PicoPure RNA Isolation Kit (Thermo Fisher Scientific, MA, USA) according to the manufacturer's protocol with the optional on-column DNase treatment. RNA integrity (RIN) was assessed by running all samples on an Agilent RNA 6000 Pico chip (Agilent Technologies, CA, USA) and three biological replicates with RIN > 7.0 were selected for further processing. Double stranded cDNA amplified using Clontech SMARTer PCR cDNA synthesis kit (634926, TaKaRa Bio USA) was fragmented for 15 min using Fragmentase (M0348, New England Biolabs) and processed into Illumina sequencing libraries as follows: the ends of 1.5X AMPure XP bead (A63880, Agencourt) purified fragmented DNA was repaired with End Repair Enzyme Mix (E6050 New England Biolabs) and Klenow DNA Polymerase (M0210, NEB), followed by dA-tailing using

638 Klenow 3'-5' exonuclease (M0212, NEB). The Illumina TruSeq universal adapter dimer
639 was ligated to library fragments with rapid T4 DNA Ligase (L6030-HC-L, Enzymatics),
640 followed by 3 rounds of 1X AMPure XP bead purification to remove unligated adapter.
641 Finally, libraries were enriched and indexed by PCR using Phusion HiFi Polymerase mix
642 (M0531, NEB). Illumina libraries were quantified using a nanodrop, pooled to a final
643 concentration of 20 nM and sequenced as single end 100 bp reads on Illumina HiSeq2500
644 at the Washington University in St. Louis School of Medicine Genome Technology
645 Access Center (https://gtac.wustl.edu/).
646
647 **RNA-Seq data analysis**
648 Adapters and low quality bases were removed using Trimmomatic (Bolger et al., 2014)
649 with default parameters. Trimmed reads were mapped to the ITAG2.3 *Solanum*
650 *lycopersicum* genome
651 (https://solgenomics.net/organism/Solanum_lycopersicum/genome; The Tomato Genome
652 Consortium, 2012) using bowtie2 (Langmead and Salzberg, 2012) to obtain SAM files.
653 After sorting and indexing of SAM files, BAM files files were generated using samtools
654 commands (Li and Handsaker et al., 2009). The BEDtools multicov tool (Quinlan and
655 Hall, 2010) was then used to obtain read counts per annotated gene for each sample.
656 Subsequent analysis was done with the R package edgeR (Robinson et al., 2010). After
657 normalization for library size 20,231 genes with at least one count per million reads
658 across three samples were retained for further analysis. Lists of Differentially Expressed
659 Genes (DEGs) were generated between pairwise sample combinations with q-value <
660 0.05. For IL2-5 and IL4-3 at P1, P3, and P4 stages, we identified genes that are
661 differentially expressed relative to M82 in both the IL and the Sp parent to interrogate
662 Sp-like changes in gene expression in the ILs. For P2, the list of DEG in each IL reflects
663 changes relative to M82 only (Supplemental Dataset 5).
664
665 **Gene Ontology, Mapman, and promoter motif enrichment analyses**
666 Lists of IL organ-specific DEGs were interrogated for enrichment of Gene Ontology
667 terms using agriGO (http://bioinfo.cau.edu.cn/agriGO/; Du et al., 2010) with default

parameters (Fisher's exact significance test and Yekutieli FDR adjustment at $q < 0.05$). We further divided DEG gene lists into IL up-regulated and down-regulated genes and report significant terms in Supplemental Dataset 6. We tested IL organ-specific DEGs for enrichment of annotated promoter motifs using a custom R script (Dr. Julin Maloof). Briefly, functions in the Bioconductor Biostrings package (Pages et al., 2016) were implemented to count the frequency of 100 known motifs in the promoters of DEGs (1000 bp upstream sequence) and calculate p-values for enrichment based on these counts. We report exact matches of known motifs and motifs with up to 1 mismatch in IL up-regulated and down-regulated organ-specific gene sets (Supplemental Dataset 7). For Mapman analysis (Thimm et al., 2004) the Slyc_ITAG2.3 v1.1 mapping was used. The $\log_2$ normalized expression of tomato genes belonging to functional categories cell cycle/cell division (Mapman bins 31.2, 31.3) and photosynthesis (Mapman bin 1) are plotted against leaf ontogeny for each genotype.

IL organ-specific gene network inference

To infer IL organ-specific networks (Figure 7A-D, Table S8), we selected DEGs between IL2-5/M82 (IL4-3/M82) and Sp/M82 for each organ (P1, P3, P4) (q value < 0.05). Since co-expression analysis can inform the likelihood that genes interact, or participate in the same functional pathway, the selected genes for each IL (IL2-5 or IL4-3) and each organ were clustered based on their co-expression across genotypes. To perform clustering, the Silhouette index (Rousseeuw, 1987) followed by K-means (MacQueen, 1967) were applied. After clustering, networks were inferred as in de Luis Balaguer and Sozzani (in press). Briefly, for each DEG, we identified a set of potential regulators and measured the likelihood of gene-target regulation using a Bayesian Dirichlet equivalence uniform (Boutine, 1991). Genes that had the highest value of the Bayesian Dirichlet equivalence uniform were chosen as regulators, and of these only transcription factors (as annotated by Suresh et al., 2014) were further considered as regulatory (source) nodes. To obtain the final IL2-5 and IL4-3 organ-specific networks, the networks for each cluster were connected. For this, we found regulations among the cluster hubs (node of each individual network with the largest degree of edges leaving the node) by using the same

Bayesian Dirichlet equivalence uniform metric. In addition, we implemented a score to estimate whether the inferred interactions were activations or repressions. The score was calculated for each edge and it measured the ratio between i) the conditional probability that a gene is expressed given that its regulator was expressed in the prior time point, and ii) the conditional probability that a gene is expressed given that its regulator was not expressed in the prior time point. If the first conditional probability is larger than the second one, then the parent was found to be an activator and *vice versa*. In the case of a tie, the edge was found to have an undetermined sign. Networks for each organ were jointly visualized in Cytoscape (Shannon et al., 2003).

Dynamic IL network construction

To infer dynamic IL networks (Figure 7E-F, Supplemental Dataset 9), we selected DEGs between IL2-5/M82 or IL4-3/M82 and Sp/M82 for each organ (P1, P3, P4) (q value < 0.05 or (FC > 2.0 and q value < 0.2)). All DEG in the IL2-5 or IL4-3 were clustered in four groups, corresponding to the four developmental stages: each gene was assigned to the developmental stage where it showed the maximum expression. A network was then inferred for each developmental stage as described for the IL organ-specific networks. To ensure that all potential regulators of each gene were considered, genes from the preceding developmental stage were included in the inference of the network of each developmental stage. The final network for each IL was visualized in Cytoscape (Shannon et al., 2003).

Accession Numbers

An NCBI SRA accession number will be provided upon publication.

Supporting Data

Supplemental Figure 1. Dual confocal profilometer device used to measure leaf thickness.

Supplemental Figure 2. Comparison of leaf thickness of select ILs in field and

greenhouse conditions.

Supplemental Figure 3. Summary of differentially expressed genes in IL2-5 and IL4-3.

Supplemental Figure 4. Expression profiles of differentially expressed putative transcription factors in ILs 2-5 and 4-3.

Supplemental Figure 5. Expression profiles of *LANCEOLATE* across leaf plastochrons P1-P4.

Supplemental Dataset 1. Trait value estimates and heritability for leaf thickness, LMA, and leaflet shape across the IL panel.

Supplemental Dataset 2. Trait value estimates and heritability for elemental concentration across the IL panel.

Supplemental Dataset 3. Summary of all measured and meta-data traits used in correlation matrix.

Supplemental Dataset 4. Pairwise trait correlation matrix including significance values.

Supplemental Dataset 5. List of differentially expressed genes ($q < 0.05$) in each organ (P1 – P4) for the comparison: (M82/IL) overlapping with (M82/*S. pennellii*).

Supplemental Dataset 6. List of significantly enriched ($q < 0.05$) Gene Ontology (GO) terms for gene sets listed in Supplemental Dataset 5.

Supplemental Dataset 7. List of enriched ($q < 0.05$) promoter motifs for gene sets in Supplemental Dataset 5.

Supplemental Dataset 8. List of organ-specific (P1, P3, P4) gene interactions for IL2-5 and IL4-3.

Supplemental Dataset 9. List of dynamic gene interactions for IL2-5 and IL4-3.

Author Contributions

VC, MHF and DHC designed the research. VC, MF, MADLB, RS, and ML conducted the experiments and analyzed the data. VC wrote the manuscript with contributions from other authors.

Acknowledgments

S. pennellii introgression line panel seeds were provided by Dr. Neelima Sinha (University of California, Davis) and the Tomato Genetics Resource Center (University of California, Davis). We would like to thank Dr. Ivan Baxter and Dr. Greg Ziegler

(Danforth Plant Science Center) for generating elemental profile data, Dr. Naomi Ori (Hebrew University of Jerusalem) for generously contributing tomato DR5::Venus seeds, and Dr. Julin Maloof (University of California, Davis) for sharing custom promoter enrichment analysis scripts. We acknowledge the advice and assistance of Dr. Noah Fahlgren, Dr. Malia Gehan, and Melinda Darnell (Danforth Plant Science Center) with drought phenotyping experiments. We thank Dr. Elizabeth Kellogg for insightful discussions and comments on the manuscript. This work was supported by funds from the Donald Danforth Plant Science Center. RS is supported by an NSF CAREER grant (MCB-1453130). MHF is supported by an NSF NPGI post-doctoral fellowship (IOS-1523668).

770 **References**

771

772 **Abràmoff, M. D., Magalhães, P. J., & Ram, S. J.** (2004). Image processing with
773 ImageJ. *Biophotonics International* **11**(7), 36-42.
774 **Andriankaja, M., Dhondt, S., De Bodt, S., Vanhaeren, H., Coppens, F., De Milde, L.,**
775 **... & Inzé, D.** (2012). Exit from proliferation during leaf development in Arabidopsis
776 thaliana: a not-so-gradual process. *Developmental Cell* **22**(1), 64-78.
777 **Becker, B.** (2007). Function and evolution of the vacuolar compartment in green algae
778 and land plants (Viridiplantae). *International Review of Cytology* **264**, 1-24.
779 **John, G. P., Scoffoni, C., & Sack, L.** (2013). Allometry of cells and tissues within
780 leaves. *American Journal of Botany* **100**(10), 1936-1948.
781 **Ben-Gera, H., Shwartz, I., Shao, M. R., Shani, E., Estelle, M., & Ori, N.** (2012).
782 ENTIRE and GOBLET promote leaflet development in tomato by modulating auxin
783 response. *The Plant Journal* **70**(6), 903-915.
784 **Bohmert, K., Camus, I., Bellini, C., Bouchez, D., Caboche, M., & Benning, C.** (1998).
785 AGO1 defines a novel locus of Arabidopsis controlling leaf development. *The EMBO*
786 *Journal* **17**(1), 170-180.
787 **Buntine, W.** 1991. Theory refinement on Bayesian networks. In *Proceedings of the*
788 *Seventh conference on Uncertainty in Artificial Intelligence*, 52-60. Morgan Kaufmann
789 Publishers Inc.
790 **Burko, Y., Shleizer-Burko, S., Yanai, O., Shwartz, I., Zelnik, I. D., Jacob-Hirsch, J.,**
791 **... & Ori, N.** (2013). A role for APETALA1/FRUITFULL transcription factors in tomato
792 leaf development. *The Plant Cell* **25**(6), 2070-2083.
793 **Chitwood, D. H., Kumar, R., Headland, L. R., Ranjan, A., Covington, M. F.,**
794 **Ichihashi, Y., ... & Sinha, N. R.** (2013). A quantitative genetic basis for leaf morphology
795 in a set of precisely defined tomato introgression lines. *The Plant Cell* **25**(7), 2465-2481.
796 **Cignoni, P., Callieri, M., Corsini, M., Dellepiane, M., Ganovelli, F., & Ranzuglia, G.**
797 (2008, July). Meshlab: an open-source mesh processing tool. In *Eurographics Italian*
798 *Chapter Conference* **2008**, 129-136.
799 **Dhondt, S., Coppens, F., De Winter, F., Swarup, K., Merks, R. M., Inzé, D., ...**

& Beemster, G. T. (2010). SHORT-ROOT and SCARECROW regulate leaf growth in Arabidopsis by stimulating S-phase progression of the cell cycle. *Plant Physiology* **154**(3), 1183-1195.

Díaz-Mendoza, M., Velasco-Arroyo, B., González-Melendi, P., Martínez, M., & Díaz, I. (2014). C1A cysteine protease–cystatin interactions in leaf senescence. *Journal of Experimental Botany* **65**(14), 3825-3833.

Du, Z., Zhou, X., Ling, Y., Zhang, Z., & Su, Z. (2010). agriGO: a GO analysis toolkit for the agricultural community. *Nucleic Acids Research* **38**, W64-W70.

Eggli, U., & Nyffeler, R. (2009). Living under temporarily arid conditions–succulence as an adaptive strategy. *Bradleya* **27**, 13-36.

Eshed, Y., & Zamir, D. (1995). An introgression line population of Lycopersicon pennellii in the cultivated tomato enables the identification and fine mapping of yield-associated QTL. *Genetics* **141**(3), 1147-1162.

Fridman, E., Carrari, F., Liu, Y. S., Fernie, A. R., & Zamir, D. (2004). Zooming in on a quantitative trait for tomato yield using interspecific introgressions. *Science* **305**(5691), 1786-1789.

Garnier, E., & Laurent, G. (1994). Leaf anatomy, specific mass and water content in congeneric annual and perennial grass species. *New Phytologist* **128**(4), 725-736.

Gibson, A. C. (1982). The anatomy of succulence. In *Crassulacean acid metabolism*. J. Proc. V ann. Symp. Bot., Univ. Calif., Riverside. *J. Amer. Soc. Plant Physiologists*: Rockville, USA, 1-17.

Gong, P., Zhang, J., Li, H., Yang, C., Zhang, C., Zhang, X., ... & Ye, Z. (2010). Transcriptional profiles of drought-responsive genes in modulating transcription signal transduction, and biochemical pathways in tomato. *Journal of Experimental Botany* **61**(13), 3563-3575.

Gonzalez, N., Vanhaeren, H., & Inzé, D. (2012). Leaf size control: complex coordination of cell division and expansion. *Trends in Plant Science* **17**(6), 332-340.

Haliński, Ł. P., Kalkowska, M., Kalkowski, M., Piorunowska, J., Topolewska, A., & Stepnowski, P. (2015). Cuticular wax variation in the tomato (Solanum lycopersicum L.), related wild species and their interspecific hybrids. *Biochemical Systematics and*

Ecology **60**, 215-224.

Hay, A., & Tsiantis, M. (2010). KNOX genes: versatile regulators of plant development and diversity. *Development* **137**(19), 3153-3165.

Holtan, H. E., & Hake, S. (2003). Quantitative trait locus analysis of leaf dissection in tomato using Lycopersicon pennellii segmental introgression lines. *Genetics* **165**(3), 1541-1550.

Huang, W., Xian, Z., Kang, X., Tang, N., & Li, Z. (2015). Genome-wide identification, phylogeny and expression analysis of GRAS gene family in tomato. *BMC Plant Biology* **15**(1), 209.

Ichihashi, Y., Aguilar-Martínez, J. A., Farhi, M., Chitwood, D. H., Kumar, R., Millon, L. V., ... & Sinha, N. R. (2014). Evolutionary developmental transcriptomics reveals a gene network module regulating interspecific diversity in plant leaf shape. *Proceedings of the National Academy of Sciences* **111**(25), E2616-E2621.

Iwata, H., & Ukai, Y. (2002). SHAPE: a computer program package for quantitative evaluation of biological shapes based on elliptic Fourier descriptors. *Journal of Heredity* **93**(5), 384-385.

John, G. P., Scoffoni, C., & Sack, L. (2013). Allometry of cells and tissues within leaves. *American Journal of Botany* **100**(10), 1936-1948.

Kalve, S., Fotschki, J., Beeckman, T., Vissenberg, K., & Beemster, G. T. (2014). Three-dimensional patterns of cell division and expansion throughout the development of Arabidopsis thaliana leaves. *Journal of Experimental Botany* **65,** 6385-6397**.**

Kimura, S., Koenig, D., Kang, J., Yoong, F. Y., & Sinha, N. (2008). Natural variation in leaf morphology results from mutation of a novel KNOX gene. *Current Biology* **18**(9), 672-677.

Koenig, D., Bayer, E., Kang, J., Kuhlemeier, C., & Sinha, N. (2009). Auxin patterns Solanum lycopersicum leaf morphogenesis. *Development* **136**(17), 2997-3006.

Koenig, D., Jiménez-Gómez, J. M., Kimura, S., Fulop, D., Chitwood, D. H., Headland, L. R., ... & Tohge, T. (2013). Comparative transcriptomics reveals patterns of selection in domesticated and wild tomato. *Proceedings of the National Academy of Sciences* **110**(28), E2655-E2662.

Kolde, R. (2015). pheatmap: Pretty Heatmaps. R package version 1.0. 2.

Kumar, R., Kushalappa, K., Godt, D., Pidkowich, M. S., Pastorelli, S., Hepworth, S. R., & Haughn, G. W. (2007). The Arabidopsis BEL1-LIKE HOMEODOMAIN proteins SAW1 and SAW2 act redundantly to regulate KNOX expression spatially in leaf margins. *The Plant Cell* **19**(9), 2719-2735.

Kuznetsova, A., Christensen, R. H., Bavay, C., & Brockhoff, P. B. (2015). Automated mixed ANOVA modeling of sensory and consumer data. *Food Quality and Preference* **40**, 31-38.

Li, H., Handsaker, B., Wysoker, A., Fennell, T., Ruan, J., Homer, N., ... & Durbin, R. (2009). The sequence alignment/map format and SAMtools. *Bioinformatics* **25**(16), 2078-2079.

Lightfoot, D. A., Mungur, R., Ameziane, R., Nolte, S., Long, L., Bernhard, K., ... & Young, B. (2007). Improved drought tolerance of transgenic Zea mays plants that express the glutamate dehydrogenase gene (gdhA) of E. coli. *Euphytica* **156**(1-2), 103-116.

McDowell, E. T., Kapteyn, J., Schmidt, A., Li, C., Kang, J. H., Descour, A., ... & Jones, A. D. (2011). Comparative functional genomic analysis of Solanum glandular trichome types. *Plant Physiology* **155**(1), 524-539.

McHale, N. A. (1992). A nuclear mutation blocking initiation of the lamina in leaves of Nicotiana syhestris. *Planta* **186**(3), 355-360.

McHale, N. A. (1993). LAM-1 and FAT genes control development of the leaf blade in Nicotiana sylvestris. *The Plant Cell* **5**(9), 1029-1038.

MacQueen, J. (1967, June). Some methods for classification and analysis of multivariate observations. In *Proceedings of the fifth Berkeley symposium on mathematical statistics and probability* **1**(14), 281-297.

Muir, C. D., Conesa, M. À., Roldán, E. J., Molins, A., & Galmés, J. (2016). Weak coordination between leaf structure and function among closely related tomato species. *New Phytologist*.

Muir, C. D., Pease, J. B., & Moyle, L. C. (2014). Quantitative genetic analysis indicates natural selection on leaf phenotypes across wild tomato species (Solanum sect.

Lycopersicon; Solanaceae). *Genetics* **198**(4), 1629-1643.

Nakazato, T., Warren, D. L., & Moyle, L. C. (2010). Ecological and geographic modes of species divergence in wild tomatoes. *American Journal of Botany* **97**(4), 680-693.

Nelson, E. A., Sage, T. L., & Sage, R. F. (2005). Functional leaf anatomy of plants with crassulacean acid metabolism. *Functional Plant Biology* **32**(5), 409-419.

Nicotra, A. B., Leigh, A., Boyce, C. K., Jones, C. S., Niklas, K. J., Royer, D. L., & Tsukaya, H. (2011). The evolution and functional significance of leaf shape in the angiosperms. *Functional Plant Biology* **38**(7), 535-552.

Niinemets, Ü., Díaz-Espejo, A., Flexas, J., Galmés, J., & Warren, C. R. (2009). Role of mesophyll diffusion conductance in constraining potential photosynthetic productivity in the field. *Journal of Experimental Botany* **60**(8), 2249-2270.

Ogburn, R., & Edwards, E. J. (2010). The ecological water-use strategies of succulent plants. *Advances in Botanical Research* **55**, 179-225.

Oguchi, R., Hikosaka, K., & Hirose, T. (2005). Leaf anatomy as a constraint for photosynthetic acclimation: differential responses in leaf anatomy to increasing growth irradiance among three deciduous trees. *Plant, Cell & Environment* **28**(7), 916-927.

Ori, N., Cohen, A. R., Etzioni, A., Brand, A., Yanai, O., Shleizer, S., ... & Alvarez, J. P. (2007). Regulation of LANCEOLATE by miR319 is required for compound-leaf development in tomato. *Nature Genetics* **39**(6), 787-791.

Pieruschka, R., & Poorter, H. (2012). Phenotyping plants: genes, phenes and machines. *Functional Plant Biology* **39**(11), 813-820.

Poorter, H., Niinemets, Ü., Poorter, L., Wright, I. J., & Villar, R. (2009). Causes and consequences of variation in leaf mass per area (LMA): a meta-analysis. *New Phytologist* **182**(3), 565-588.

Preston, J. C., & Hileman, L. (2013). Functional evolution in the plant SQUAMOSA-PROMOTER BINDING PROTEIN-LIKE (SPL) gene family. *Frontiers in Plant Science* **4**, 80.

Quinlan, A. R., & Hall, I. M. (2010). BEDTools: a flexible suite of utilities for comparing genomic features. *Bioinformatics* **26**(6), 841-842.

Ranjan, A., Budke, J., Rowland, S. D., Chitwood, D. H., Kumar, R., Carriedo, L. G.,

... & Sinha, N. (2016). eQTL regulating transcript levels associated with diverse biological processes in tomato. *Plant Physiology* **172**, 328-340.

de Reuille, P. B., Routier-Kierzkowska, A. L., Kierzkowski, D., Bassel, G. W., Schüpbach, T., Tauriello, G., ... & Burian, A. (2015). MorphoGraphX: a platform for quantifying morphogenesis in 4D. *Elife* **4**, e05864.

Robinson, M. D., McCarthy, D. J., & Smyth, G. K. (2010). edgeR: a Bioconductor package for differential expression analysis of digital gene expression data. *Bioinformatics* **26**(1), 139-140.

Roderick, M. L., Berry, S. L., Noble, I. R., & Farquhar, G. D. (1999). A theoretical approach to linking the composition and morphology with the function of leaves. *Functional Ecology* **13**(5), 683-695.

Rousseeuw, P. J. (1987). Silhouettes: a graphical aid to the interpretation and validation of cluster analysis. *Journal of Computational and Applied Mathematics* **20**, 53-65.

Rustamov, R. M. (2007, July). Laplace-Beltrami eigenfunctions for deformation invariant shape representation. In *Proceedings of the fifth Eurographics symposium on Geometry processing*, 225-233. Eurographics Association.

Sack, L., & Frole, K. (2006). Leaf structural diversity is related to hydraulic capacity in tropical rain forest trees. *Ecology* **87**(2), 483-491.

Schauer, N., Semel, Y., Roessner, U., Gur, A., Balbo, I., Carrari, F., ... & Willmitzer, L. (2006). Comprehensive metabolic profiling and phenotyping of interspecific introgression lines for tomato improvement. *Nature Biotechnology* **24**(4), 447-454.

Semel, Y., Nissenbaum, J., Menda, N., Zinder, M., Krieger, U., Issman, N., ... & Zamir, D. (2006). Overdominant quantitative trait loci for yield and fitness in tomato. *Proceedings of the National Academy of Sciences* **103**(35), 12981-12986.

Shannon, P., Markiel, A., Ozier, O., Baliga, N. S., Wang, J. T., Ramage, D., ... & Ideker, T. (2003). Cytoscape: a software environment for integrated models of biomolecular interaction networks. *Genome Research* **13**(11), 2498-2504

Shleizer-Burko, S., Burko, Y., Ben-Herzel, O., & Ori, N. (2011). Dynamic growth program regulated by LANCEOLATE enables flexible leaf patterning. *Development* **138**(4), 695-704.

950 **Smith, S. D., Monson, R. K., & Anderson, J. E.** (1997). Plant processes and responses
951 to stress. In *Physiological Ecology of North American Desert Plants*, 45-71. Springer
952 Berlin Heidelberg.
953 **Suresh, B. V., Roy, R., Sahu, K., Misra, G., & Chattopadhyay, D.** (2014). Tomato
954 genomic resources database: an integrated repository of useful tomato genomic
955 information for basic and applied research. *PLoS One* **9**(1), e86387.
956 **Taji, T., Ohsumi, C., Iuchi, S., Seki, M., Kasuga, M., Kobayashi, M., ... & Shinozaki,**
957 **K.** (2002). Important roles of drought□and cold□inducible genes for galactinol synthase
958 in stress tolerance in Arabidopsis thaliana. *The Plant Journal* **29**(4), 417-426.
959 **Terashima, I., Hanba, Y. T., Tholen, D., & Niinemets, Ü.** (2011). Leaf functional
960 anatomy in relation to photosynthesis. *Plant Physiology* **155**(1), 108-116.
961 **Thimm, O., Bläsing, O., Gibon, Y., Nagel, A., Meyer, S., Krüger, P., ... & Stitt, M.**
962 (2004). Mapman: a user-driven tool to display genomics data sets onto diagrams of
963 metabolic pathways and other biological processes. *The Plant Journal* **37**(6), 914-939.
964 **Tomato Genome Consortium.** (2012). The tomato genome sequence provides insights
965 into fleshy fruit evolution. *Nature* **485**(7400), 635-641.
966 **Tsuge, T., Tsukaya, H., & Uchimiya, H.** (1996). Two independent and polarized
967 processes of cell elongation regulate leaf blade expansion in Arabidopsis thaliana (L.)
968 Heynh. *Development* **122**(5), 1589-1600.
969 **Tsukaya, H.** (2003). Organ shape and size: a lesson from studies of leaf morphogenesis.
970 *Current Opinion in Plant Biology* **6**(1), 57-62.
971 **Wickham, H.** (2009). ggplot2: elegant graphics for data analysis. Springer New York
972 **1**(2), 3.
973 **von Willert, D. J.** (1992). *Life strategies of succulents in deserts: with special reference*
974 *to the Namib Desert*. CUP Archive.
975 **Wright, I. J., Reich, P. B., Westoby, M., Ackerly, D. D., Baruch, Z., Bongers, F., ... &**
976 **Flexas, J.** (2004). The worldwide leaf economics spectrum. *Nature* **428**(6985), 821-827.
977 **Wuyts, N., Massonnet, C., Dauzat, M., & Granier, C.** (2012). Structural assessment of
978 the impact of environmental constraints on Arabidopsis thaliana leaf growth: a 3D
979 approach. *Plant, Cell & Environment* **35**(9), 1631-1646.

Ziegler, G., Terauchi, A., Becker, A., Armstrong, P., Hudson, K., & Baxter, I. (2013). Ionomic screening of field-grown soybean identifies mutants with altered seed elemental composition. *The Plant Genome* **6**(2).

983 **Figure Legends**

984

985 **Figure 1. Desert-adapted tomato plants have thicker leaves than domesticated**
986 **tomato and are resistant to drought. (A)** Thickness across leaflet blades of
987 domesticated (*S. lycopersicum*, M82) and desert-adapted (*S. pennellii*) tomatoes
988 measured with a custom-built dual confocal profilometer device (Supplemental Figure 1).
989 Median thickness of the *S. lycopersicum* leaflet shown here is 211 μm, and 294 μm for *S.*
990 *pennellii*. (**B**) Confocal images of propidium iodide stained leaflet cross-sections; scale
991 bar is 200 μm. (**C**) Total shoot area normalized by taking the square root of pixels from
992 top view phenotyping images over 16 days in three water treatments (n=8). Gray shading
993 reflects standard error.

994

995 **Figure 2. Quantitative Trait Loci for leaf thickness and circularity in tomato.** Leaflet
996 thickness **(A)** and circularity **(B)** values across the *S. pennellii* introgression line panel.
997 Colors indicate level of significance in comparisons of each IL with M82 (arrow). **(C)**
998 Significant correlations (Spearman's rho) between leaf thickness (LT), or leaf mass per
999 area (LMA) and a suite of other traits across the *S. pennellii* IL panel ($q < 0.05$). Traits
1000 are grouped by type: ION, elemental profile; MOR, morphological; DEV, developmental;
1001 ENZ, enzyme activity; SED, seed metabolite content (Supplemental Datasets 3 and 4).

1002

1003 **Figure 3. Anatomical manifestations of thicker leaves**. (**A**) Confocal images of
1004 propidium iodide stained cross-sections of field-grown M82 and select ILs; Sp, *S.*
1005 *pennellii* grown in greenhouse conditions; scale bars are 50 microns. **(B)** Representative
1006 leaf thickness plots and **(C)** leaflet binary images of field-grown plants as for (A). **(D-F)**
1007 3D confocal projections of vegetative shoot apices of **(D)** M82, **(E)** IL2-5, and **(F)** IL4-3
1008 plants carrying a DR5::Venus construct; green fluorescence, Venus fluorophore; red
1009 fluorescence, chlorophyll; scale bars, 200 μm; arrows point to DR5 promoter-driven
1010 Venus fluorescence at the tips of P3 leaflet primordia. **(G)** P3 organ volume (log_2
1011 normalized), length, and mean diameter calculated from 3D surface reconstructions (n =
1012 9; asterisk indicates significant difference relative to M82 * $p < 0.05$, ** $p < 0.01$).

Figure 4. Comparative transcriptomics of leaf development in thick ILs and their parents. (A) Successive stages of leaf development (plastochrons P1-P4 colored according to legend on right) were dissected from M82, *S. pennellii* (Sp) and thick ILs 2-5 and 4-3. **(B)** Principal Components Analysis (PCA) of normalized RNA-Seq read counts. (**C-D**) Scaled expression profiles for differentially expressed genes (DEG, $q < 0.05$) in each thick IL relative to M82. The overlap in DEGs between IL/M82 and Sp/M82 at each organ stage were selected to highlight similarities between thick ILs and the Sp parent. (**E**) Scaled expression profiles of differentially expressed transcription factors common to thick ILs 2-5 and 4-3. IL plastochron stages with statistically significant differential expression ($q < 0.05$) relative to M82 are marked with an asterisk.

Figure 5. Cell cycle and photosynthesis related transcript accumulation profiles. Normalized expression of cell cycle/cell division (Mapman bins 31.2, 31.3) and photosynthesis (Mapman bin 1) associated genes across plastochrons P1-P4 of ILs 2-5 and 4-3 relative to M82. Grey shaded areas denote 95 % confidence intervals.

Figure 6. Summary of statistically enriched promoter motifs among the lists of DEGs in each thick IL. The total number and general classes of significantly enriched motifs in a given category is indicated. Broad categories are color-coded and include motifs that are associated with regulation of expression by abiotic factors such as light, dehydration, and temperature, or by endogenous processes such as development, hormone, circadian clock, or the cell cycle (Supplemental Dataset 7).

Figure 7. Dynamic Bayesian Networks of gene expression across early leaf ontogeny. Combined P1-P4 gene regulatory networks for **(A-B)** IL2-5 and **(C-D)** IL4-3. Interactions were determined within organ-specific DEGs and then combined. Overall genotype-specific network topologies are shown in **(A)** and **(C)**. Sub-networks for regulators central to more than one plastochron stage are shown in **(B)** and **(D)**. Nodes and edges are colored according to legend. **(E)** and **(F)** Sub-networks of dynamic gene regulatory

networks for IL2-5 and IL4-3, respectively, showing interactions of an AUX/IAA TF (AUX/IAA 12g, Solyc12g096980) with other source nodes. Gene IDs of highlighted nodes: SBP-box 04g, Solyc04g064470; BEL1-like 04g, Solyc04g080780; GRAS 08g, Solyc08g014030; Myb 07g, Solyc07g052490; WRKY 05g, Solyc05g015850; AUX/IAA 06g, Solyc06g008580; Myb 03g, Solyc03g005570; Myb 08g, Soly08g005870; WRKY 02g, Solyc02g080890.

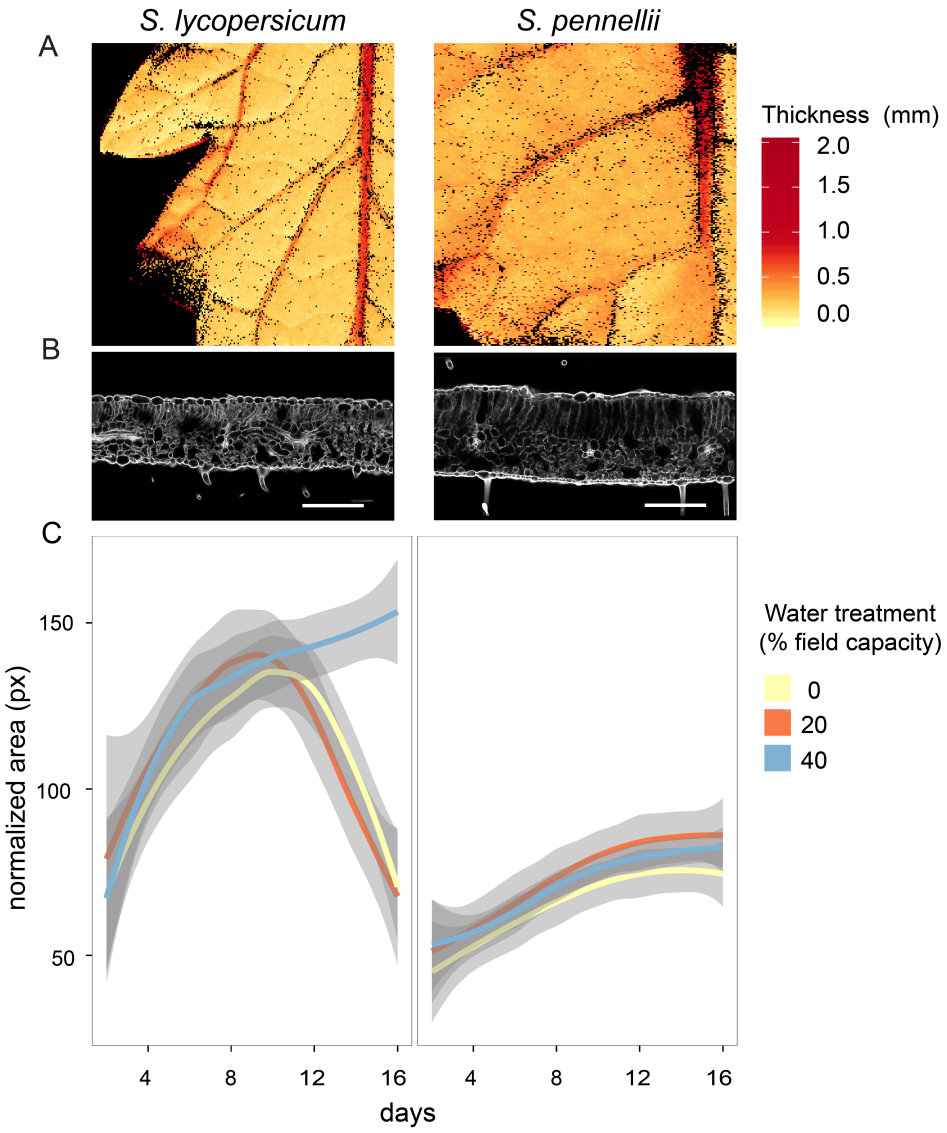

Figure 1. Desert-adapted tomato plants have thicker leaves than domesticated tomato and are resistant to drought. **(A)** Thickness across leaflet blades of domesticated (*S. lycopersicum*) and desert-adapted (*S. pennellii*) tomatoes measured with a custom-built dual confocal profilometer device (Supplemental Figure 1). Median thickness of the *S. lycopersicum* leaflet shown here is 211 µm, and 294 µm for *S. pennellii*. **(B)** Confocal images of propidium iodide stained leaflet cross-sections; scale bar is 200 µm. **(C)** Total shoot area normalized by taking the square root of pixels from top-view phenotyping images taken over 16 days in three water treatments (n=8). Gray shading around each colored line reflects standard error.

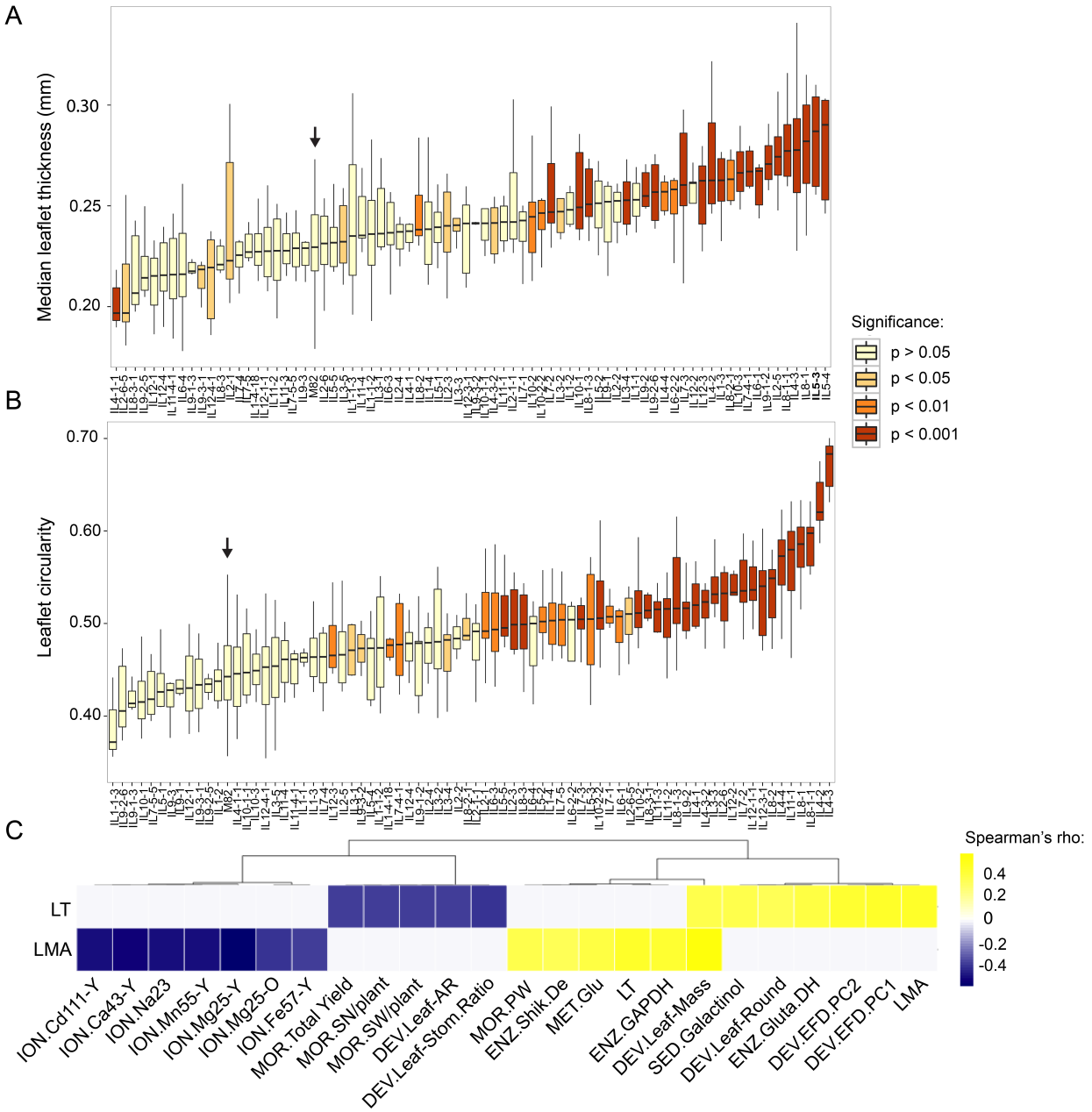

Figure 2. Leaflet thickness **(A)** and circularity **(B)** values across the *S. pennellii* introgression line panel. Colors indicate level of significance in comparisons of each IL with M82 (arrow). **(C)** Significant correlations (Spearman's rho) between leaf thickness (LT), or leaf mass per area (LMA) and a suite of other traits across the S. pennellii IL panel ($q < 0.05$). Traits are grouped by type: ION, elemental profile; MOR, morphological; DEV, developmental; ENZ, enzyme activity; SED, seed metabolite content (Supplemental Datasets 3 and 4).

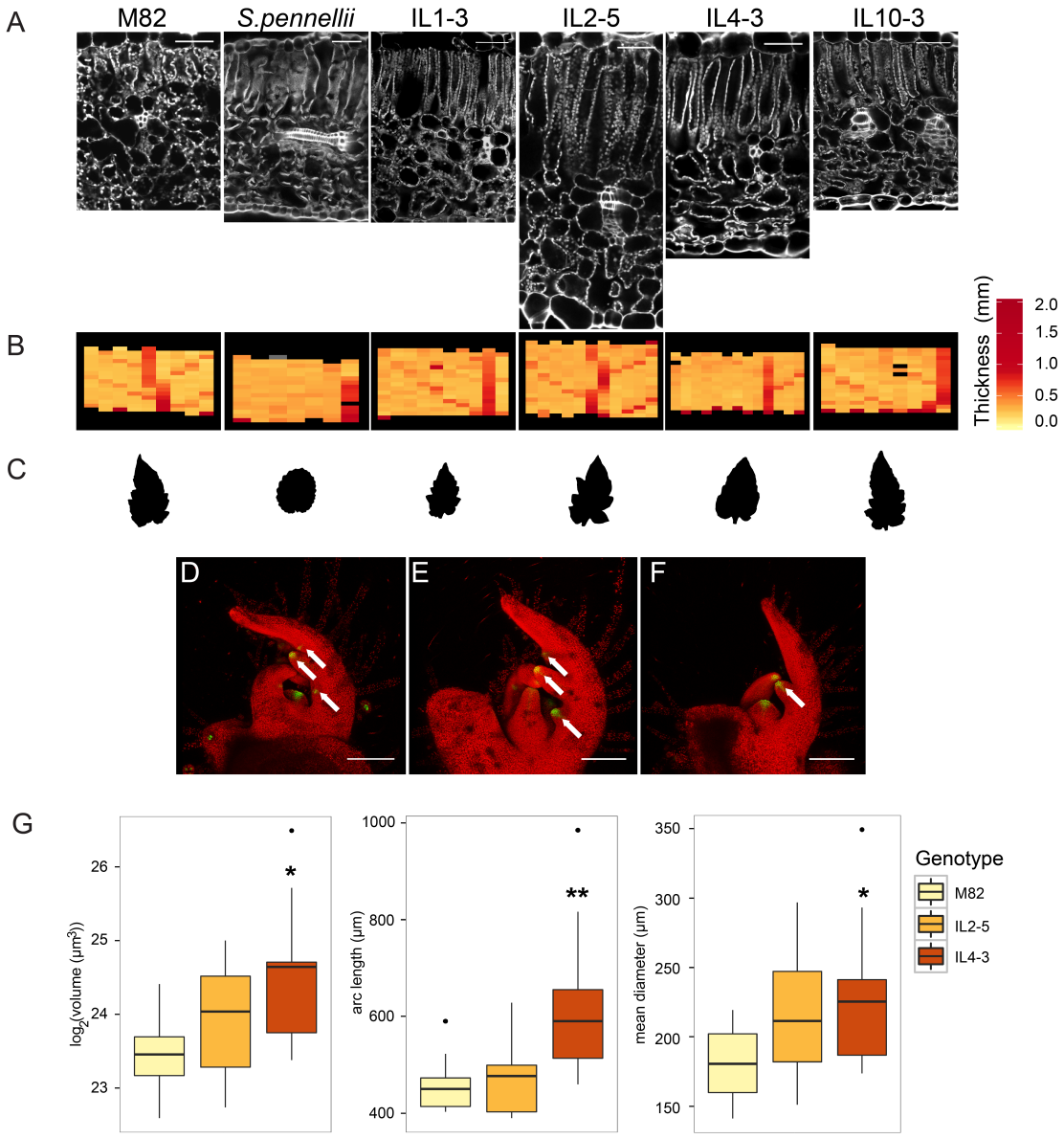

Figure 3. Anatomical manifestations of thicker leaves: **(A)** Confocal images of propidium iodide stained cross-sections of field-grown M82 and select ILs; Sp, *S. pennellii* grown in greenhouse conditions; scale bars are 50 µm. **(B)** Representative leaf thickness plots and **(C)** leaflet binary images of field-grown plants as for (A). **(D-F)** 3D confocal projections of vegetative shoot apices of **(D)** M82, **(E)** IL2-5, and **(F)** IL4-3 plants carrying a DR5::Venus construct; green fluorescence, Venus fluorophore; red fluorescence, chlorophyll; scale bars, 200 µm; arrows point to DR5 promoter-driven Venus fluorescence at the tips of P3 leaflet primordia. **(G)** P3 organ volume (log2 normalized), length, and mean diameter calculated from 3D surface reconstructions (n = 9; asterisks indicate significant difference relative to M82 * $p < 0.05$, ** $p < 0.01$).

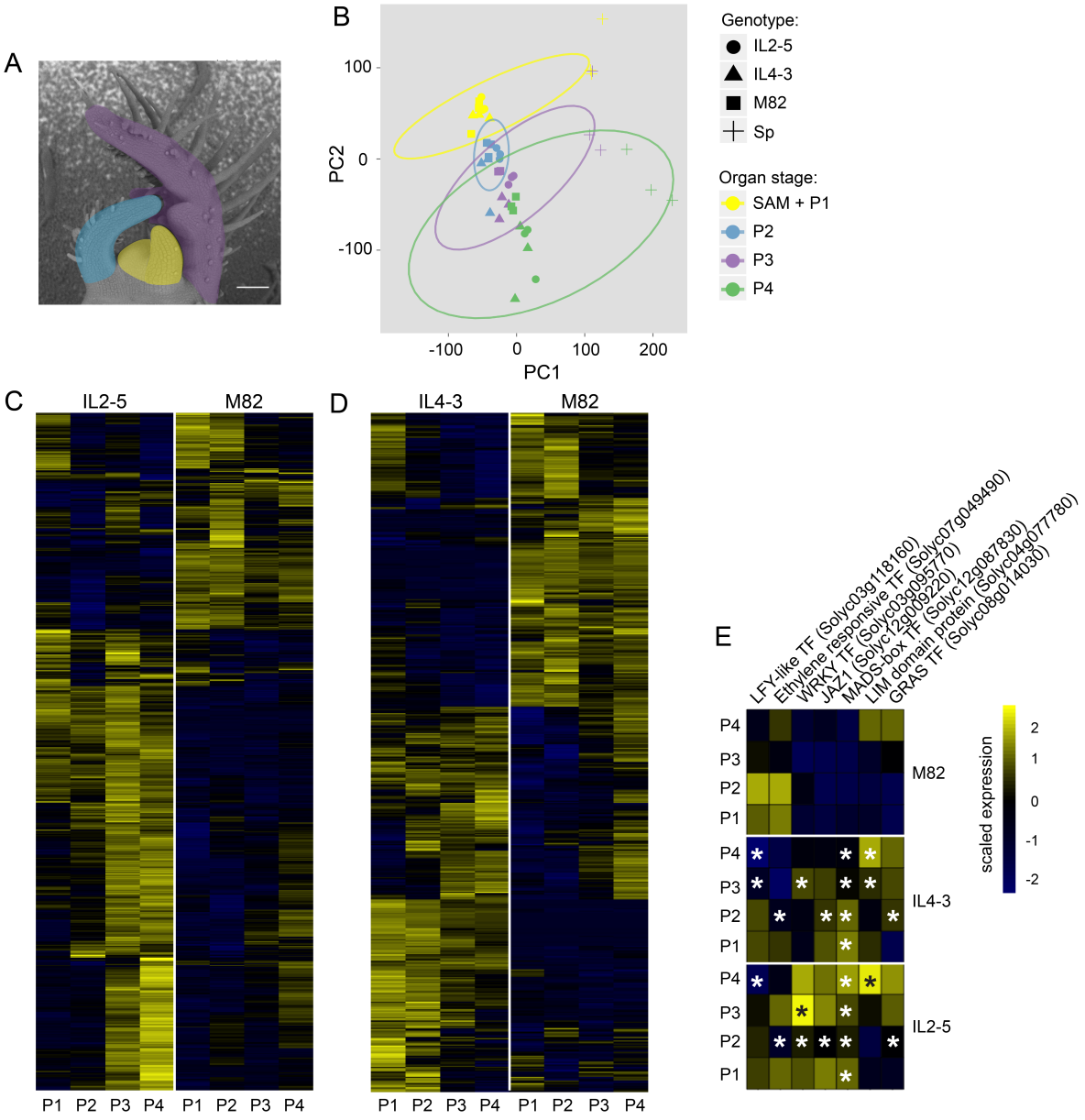

Figure 4. Comparative transcriptomics of leaf development in thick ILs and their parents. **(A)** Successive stages of leaf development (plastochrons P1-P4 colored according to legend on right) were dissected from M82, *S. pennellii* (Sp) and thick ILs 2-5 and 4-3. **(B)** Principal Components Analysis (PCA) of normalized RNA-Seq read counts. **(C-D)** Scaled expression profiles for differentially expressed genes (DEG, $q < 0.05$) in each thick IL relative to M82. The overlap in DEGs between IL/M82 and Sp/M82 at each organ stage were selected to highlight similarities between thick ILs and the Sp parent. **(E)** Scaled expression profiles of differentially expressed transcription factors common to thick ILs 2-5 and 4-3. IL plastochron stages with statistically significant differential expression ($q < 0.05$) relative to M82 are marked with an asterisk.

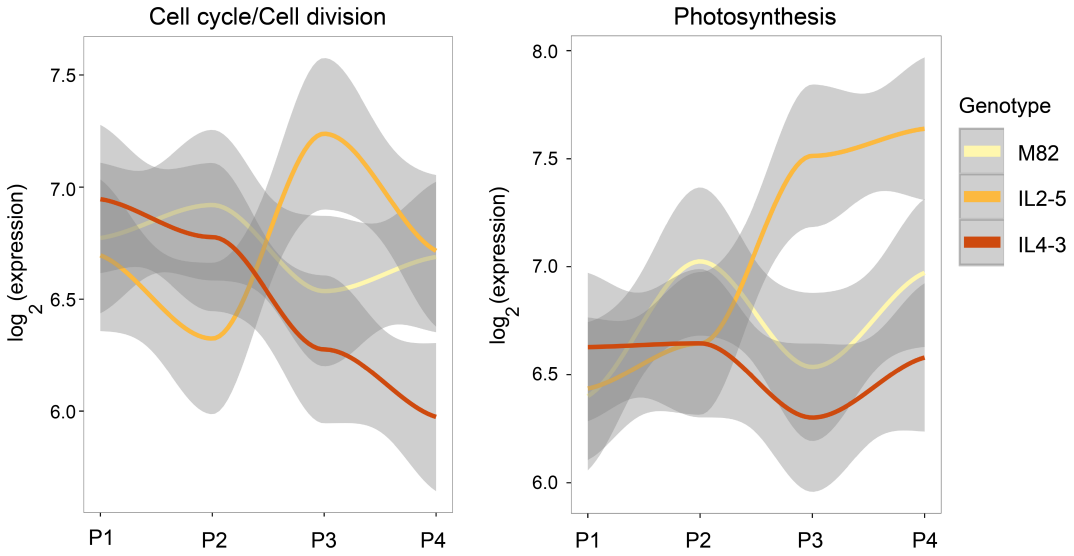

Figure 5. Normalized expression of cell cycle/cell division (Mapman bins 31.2, 31.3) and photosynthesis (Mapman bin 1) associated genes across plastochrons P1-P4 of ILs 2-5 and 4-3 relative to M82. Grey shaded areas denote 95% confidence intervals.

Genotype	Motif(s)	Num. sign. motifs	Regulation
IL2-5	SORLIP, SORLREP, G-box, PI, Ibox, ACE, TGA1, RY	31	Light
	BELL, SBP-box, ATHB, RAV1-B, ERF1, CArG, L1	14	Development
	ERE, CCA1, EveningElement	14	Circadian clock
	ABRE, ABF, DRE	12	Dehydration
	ARF, JASE	5	Hormone
	HSE, CBF2	7	Temperature
	MYB, GATA	6	Various
	E2F, MSA	2	Cell cycle
IL4-3	SORLIP, SORLREP3, G-box, Ibox, RY	9	Light
	BELL, SBP-box, CArG, AG, RAV1-A	8	Development
	CCA1, EveningElement	3	Circadian clock
	ABRE	3	Dehydration
	MYB	1	Various
	E2F	1	Cell cycle

Figure 6. Summary of statistically enriched promoter motifs among the lists of DEGs in each thick IL. The total number and general classes of significantly enriched motifs in a given category is indicated. Broad categories are color-coded and include motifs that are associated with regulation of expression by abiotic factors such as light, dehydration, and temperature, or by endogenous processes such as development, hormone, circadian clock, or the cell cycle (Supplemental Dataset 7).

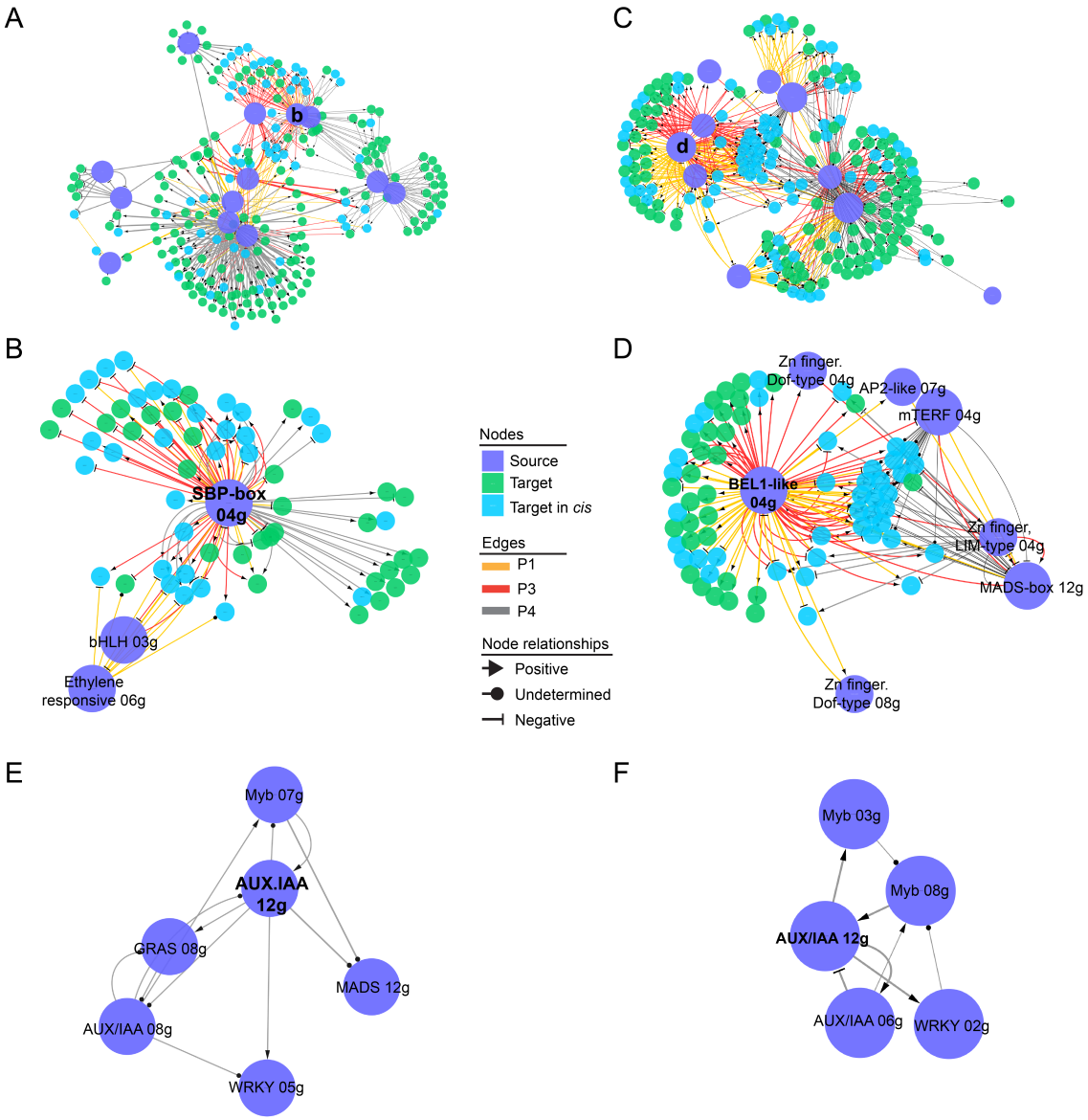

Figure 7. Combined P1-P4 gene regulatory networks for **(A-B)** IL2-5 and **(C-D)** IL4-3. Interactions were determined within organ-specific DEGs and then combined. Overall genotype-specific network topologies are shown in **(A)** and **(C)**. Sub-networks for regulators central to more than one plastochron stage are shown in **(B)** and **(D)**. Nodes and edges are colored according to legend. **(E)** and **(F)** Sub-networks of dynamic gene regulatory networks for IL2-5 and IL4-3, respectively, showing interactions of an AUX/IAA TF (AUX/IAA 12g, Solyc12g096980) with other source nodes. Gene IDs of highlighted nodes: SBP-box 04g, Solyc04g064470; BEL1-like 04g, Solyc04g080780; GRAS 08g, Solyc08g014030; Myb 07g, Solyc07g052490; WRKY 05g, Solyc05g015850; AUX/IAA 06g, Solyc06g008580; Myb 03g, Solyc03g005570; Myb 08g, Soly08g005870; WRKY 02g, Solyc02g080890.